

Regular article

Enhancement of thermoelectric efficiency in Bi_2Te_3 via rare earth element doping

Oleg Ivanov ^{*}, Maxim Yaprntsev, Roman Lyubushkin, Oxana Soklakova

Belgorod State University, Pobedy St., 85, 308015 Belgorod, Russian Federation



ARTICLE INFO

Article history:

Received 16 August 2017

Accepted 10 November 2017

Available online 20 November 2017

Keywords:

Bi_2Te_3 compound

Thermoelectric efficiency

Element doping

Rare earth elements

ABSTRACT

The Bi_2Te_3 , $\text{Bi}_{1.9}\text{Lu}_{0.1}\text{Te}_3$ and $\text{Bi}_{1.9}\text{Tm}_{0.1}\text{Te}_3$ thermoelectrics of *n*-type conductivity were prepared by microwave-solvothermal method and spark plasma sintering. At the Lu and Tm doping, the Seebeck coefficient increases, while the specific electrical conductivity and total thermal conductivity decreases resulting in thermoelectric efficiency enhancement of Bi_2Te_3 . It is believed that the thermoelectric efficiency can enhance mainly due to formation of narrow impurity Lu or Tm band with high and sharp density of states near the Fermi level. Both increase of the density-of-states effective mass of electrons and decrease of electronic contribution to the total thermal conductivity take place in this case.

© 2017 Acta Materialia Inc. Published by Elsevier Ltd. All rights reserved.

Thermoelectric materials convert energy between heat and electricity. The energy conversion efficiency is characterized by the dimensionless thermoelectric figure-of-merit, ZT , defined as $(S^2/\rho k)T$, where T , S , ρ and k are the absolute temperature, Seebeck coefficient, specific electrical resistivity and total thermal conductivity with contributions from the lattice and charge carriers [1]. At present, Bi_2Te_3 and Bi_2Te_3 -based alloys are the best materials for thermoelectric applications at temperatures around room temperature [2–4]. Unfortunately, the thermoelectric efficiency of these materials remained too low until now ($ZT \approx 1$). To improve the thermoelectric performance of Bi_2Te_3 , an element doping is often and fruitfully applied [5–10]. Of elements working as dopants, rare earth elements are the most interesting and promising doping atoms in the Bi_2Te_3 lattice. According to theoretical predictions, the thermoelectric efficiency will increase in material with a high and sharp density of states (DOS) near the Fermi level due to forming the impurity band [11–13]. In this case, both increase of S and decrease of k resulting to enhancement of ZT are expected. Before, this doping effect was successfully used to explain the ZT improving in TI-doped PbTe [14]. The ideal electronic DOS to maximize the thermoelectric efficiency is the Dirac delta function not achievable in real materials. However, electronic f -levels of rare earth elements (R) are tightly bound in atoms, and bind little in solids [15]. They give the sharp Lorentzian singularity of very narrow width in DOS near the Fermi level. This is the closest approximation to the Dirac delta function. So, the thermoelectric efficiency enhancement of Bi_2Te_3 can take place at the R -doping. Recently it was

found that rare earth elements ($R = \text{Lu}, \text{Ce}, \text{Sm}, \text{Er}, \text{La}, \text{etc.}$) can really be used as dopants to remarkably enhance the thermoelectric performance of Bi_2Te_3 [16–23]. However, it is not known at present whether enhancement of ZT is related to forming the impurity band with the high and sharp DOS.

So, the aim of this paper is to find any features in the thermoelectric properties of Lu- or Tm-doped Bi_2Te_3 related to forming the special impurity band mentioned above.

The Bi_2Te_3 , $\text{Bi}_{1.9}\text{Lu}_{0.1}\text{Te}_3$ and $\text{Bi}_{1.9}\text{Tm}_{0.1}\text{Te}_3$ compounds were prepared by the microwave-solvothermal method and spark plasma sintering. In brief, analytically pure chemicals were used for the synthesis (Bi_2O_3 , TeO_2 , Lu_2O_3 , Tm_2O_3 , ethylene glycol, nitric acid and N,N -dimethylformamide). The oxides taken in a stoichiometric ratio for each compound were dissolving in mixture of concentrated nitric acid and ethylene glycol. Then N,N -dimethylformamide was added in mixture after dissolving. The microwave-assisted reaction was carried out in a MARS-6 microwave reactor, with power of 1000 W at 2.45 MHz working frequency. The synthesis was carried out for 15 min at temperature of 463 K and pressure of 40 bars. Spark plasma sintering method by using a SPS-25/10 system was applied to sinter bulk materials at pressure of 40 MPa, temperature of 683 K and sintering time of 5 min.

The XRD patterns for the bulk Bi_2Te_3 , $\text{Bi}_{1.9}\text{Lu}_{0.1}\text{Te}_3$ and $\text{Bi}_{1.9}\text{Tm}_{0.1}\text{Te}_3$ compounds taken by a Rigaku Ultima IV diffractometer are shown in Fig. 1.

All sintered materials are single hexagonal $R\bar{3}m$ phase characteristic for pure Bi_2Te_3 . The Lu and Tm atoms entering the Bi_2Te_3 lattice change the lattice a and c parameters calculated by the Rietveld refinement (Table 1). The changes of the a and c parameters are very small and close to accuracy of the XRD analysis. Weakness of the doping effect

^{*} Corresponding author.

E-mail address: Ivanov.Oleg@bsu.edu.ru (O. Ivanov).

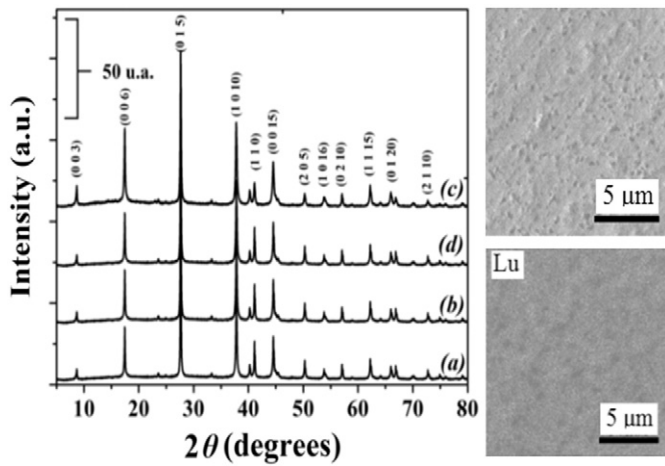


Fig. 1. XRD patterns of Bi_2Te_3 (a), $\text{Bi}_{1.9}\text{Lu}_{0.1}\text{Te}_3$ (b) and $\text{Bi}_{1.9}\text{Tm}_{0.1}\text{Te}_3$ (c) and EBSD mapping of Lu on the $\text{Bi}_{1.9}\text{Lu}_{0.1}\text{Te}_3$ surface.

on the lattice parameters can be attributed to a small difference between the atomic radii of Lu (1.75 Å), Tm (1.75 Å) and Bi (1.60 Å) [24].

The compositions of all the compounds were analyzed by an ICP-9000 emission spectrometer. Content of various elements really corresponds to the Bi_2Te_3 , $\text{Bi}_{1.9}\text{Lu}_{0.1}\text{Te}_3$ and $\text{Bi}_{1.9}\text{Tm}_{0.1}\text{Te}_3$ compositions (Table 1).

To confirm the uniformity of Lu or Tm distribution, energy dispersive X-ray spectroscopy (EDS) method was carried out. According to EDS mapping, these elements are homogeneously distributed as shown, for instance, for $\text{Bi}_{1.9}\text{Lu}_{0.1}\text{Te}_3$ (Fig. 1).

According to the Hall effect study, the majority charge carriers for all the compounds are electrons. The electron concentration, n , and Hall mobility, μ_H , values of the majority charge carriers taken at room temperature are collected in Table 2.

It is known [8,9] that the type and carrier concentration of Bi_2Te_3 is closely related to point defects. The most common defects are vacancies at the Te sites (V_{Te} , provides two electrons per defect), vacancies at the Bi sites (V_{Bi} , contributes three holes per defect) and antisite defects of Bi at the Te sites (Bi_{Te} , is accompanied with formation of one hole). For polycrystalline Bi_2Te_3 , the dangling bonds at grain boundaries due to Te deficiencies can also be considered as fractional- V_{Te} acting as n -type dopants in the same manner as whole- V_{Te} defects inside the grains. So, polycrystalline undoped Bi_2Te_3 is n -type semiconductor due to dangling bonds at grain boundaries and V_{Te} vacancies.

According to Table 2, the Lu or Tm doping results in both increase of n and decrease of μ_H . The doping effect on n can be related to the difference of electronegativity for elements forming the antisite Bi_{Te} defects responsible for formation of holes. The electronegativity values are equal to 2.1, 2.02, 1.27 and 1.25 for Te, Bi, Lu and Tm, respectively. So, larger electronegative difference for the Lu-Te and Tm-Te pairs compared to the Bi-Te pair will decrease the concentration of antisite defects at the Te-sites which contributes one hole per defect and hence result in more electrons. It is important to note that electronegativity values are very close for Lu and Tm. In this case, the electron concentration for the

Table 1
The lattice parameters and elemental compositions of Bi_2Te_3 , $\text{Bi}_{1.9}\text{Lu}_{0.1}\text{Te}_3$ and $\text{Bi}_{1.9}\text{Tm}_{0.1}\text{Te}_3$.

Compound	a , Å	c , Å	Bi, at.%	Te, at.%	Lu, at.%	Tm, at.%
Bi_2Te_3	4.385	30.476	59.87	40.13	–	–
$\text{Bi}_{1.9}\text{Tm}_{0.1}\text{Te}_3$	4.387	30.484	59.92	38.12	–	1.96
$\text{Bi}_{1.9}\text{Lu}_{0.1}\text{Te}_3$	4.388	30.481	59.95	38.07	1.98	–

Table 2

The concentration, Hall mobility and density-of-state effective mass of the majority charge carriers in Bi_2Te_3 , $\text{Bi}_{1.9}\text{Lu}_{0.1}\text{Te}_3$ and $\text{Bi}_{1.9}\text{Tm}_{0.1}\text{Te}_3$.

Compound	n , 10^{19} , cm^{-3}	μ_H , $\text{cm}^2 \text{V}^{-1} \text{s}^{-1}$	m^*
Bi_2Te_3	1.2	420	$0.16m_0$
$\text{Bi}_{1.9}\text{Tm}_{0.1}\text{Te}_3$	2.3	300	$0.25m_0$
$\text{Bi}_{1.9}\text{Lu}_{0.1}\text{Te}_3$	2.4	360	$0.25m_0$

$\text{Bi}_{1.9}\text{Lu}_{0.1}\text{Te}_3$ and $\text{Bi}_{1.9}\text{Tm}_{0.1}\text{Te}_3$ compounds should be really very close (Table 2).

Reducing the carrier mobility for Lu- and Tm-doped Bi_2Te_3 can be originated from alloy scattering of carriers [25,26]. The alloy scattering is related to forming the point defects in the Bi_2Te_3 lattice as a result of substituting the Lu and Tm atoms for the Bi site. The difference in μ_H for $\text{Bi}_{1.9}\text{Lu}_{0.1}\text{Te}_3$ and $\text{Bi}_{1.9}\text{Tm}_{0.1}\text{Te}_3$ cannot be attributed to various ionic radii of the Lu^{3+} and Tm^{3+} ions because these radii are very close. But, Tm^{3+} has a magnetic moment equal to $7\mu_B$ (μ_B is the Bohr magneton), while Lu^{3+} has zero magnetic moment. Hence, an additional electron scattering by magnetic moments of Tm^{3+} can be believed to be responsible for decrease of μ in addition to the alloy scattering. Then, μ_H of $\text{Bi}_{1.9}\text{Tm}_{0.1}\text{Te}_3$ should be lower compared to μ_H of $\text{Bi}_{1.9}\text{Lu}_{0.1}\text{Te}_3$.

The $\rho(T)$ dependences for Bi_2Te_3 , $\text{Bi}_{1.9}\text{Lu}_{0.1}\text{Te}_3$ and $\text{Bi}_{1.9}\text{Tm}_{0.1}\text{Te}_3$ measured by a ZEM-3 system within the 285–300 K range are presented in Fig. 2.

As is seen, ρ of all three compounds increases with increasing temperature. This behavior is characteristic of a degenerate semiconductor. The electrical resistivity of solids is expressed as $\rho = 1/(en\mu)$, where e is the charge of electron. The $\rho(T)$ behavior of the degenerate semiconductor is determined by T -dependent contribution from μ , while contribution from n is T -independent. The electron mobility due to phonon

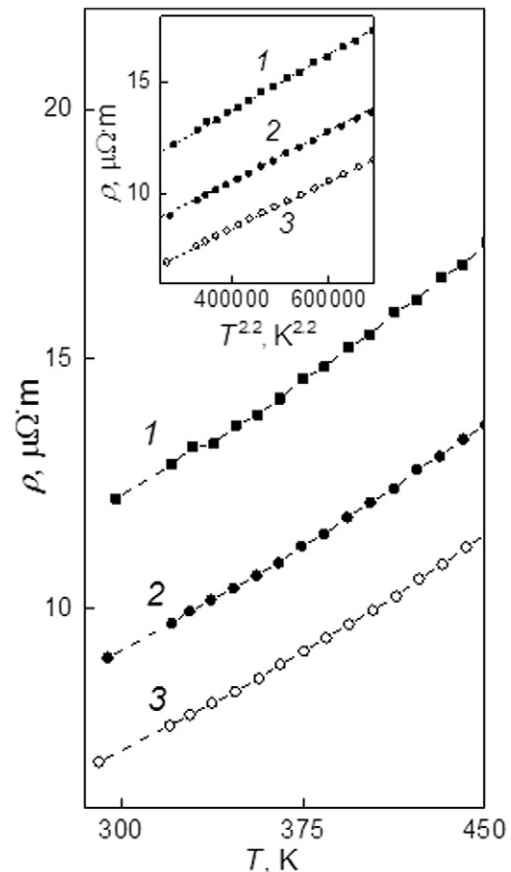


Fig. 2. The $\rho(T)$ dependences for Bi_2Te_3 (curve 1), $\text{Bi}_{1.9}\text{Tm}_{0.1}\text{Te}_3$ (2) and $\text{Bi}_{1.9}\text{Lu}_{0.1}\text{Te}_3$ (3). Inset: the $\rho(T^{2.2})$ dependences for the same compounds.

scattering of carriers usually varies as $\mu \sim T^{-m}$, where m is an exponent changing from 1.5 up to 2.5 [27]. For acoustic phonon scattering acting as main scattering mechanism at low temperatures, m is equal to -1.5 . Above the Debye temperature, optical phonon scattering becomes comparable to acoustic phonon scattering and m increases towards 2.5. For instance, the electron mobility for n -type silicon varies as $T^{-2.3}$ when both optical and acoustic phonon scattering become dominant.

According to inset to Fig. 2, the best fit for the experimental $\rho(T)$ curves corresponds to $m = 2.2$. Thus, the scattering mechanism is the same for all the compounds.

The $S(T)$ dependences for Bi_2Te_3 , $\text{Bi}_{1.9}\text{Lu}_{0.1}\text{Te}_3$ and $\text{Bi}_{1.9}\text{Tm}_{0.1}\text{Te}_3$ are presented in Fig. 3(a). Since the majority charge carries are electrons, the Seebeck coefficient has a negative sign. All of the $S(T)$ curves are really parallel to each other and linearly increase with increasing temperature.

It is known [16] that the Seebeck coefficient of the degenerate semi-conductors can be expressed as.

$$S = \frac{2k_B^2 T m^*}{3e h^2} \left(\frac{\pi}{3n}\right)^{2/3} \left(\frac{3}{2} + \gamma\right) \quad (1)$$

where k_B is the Boltzmann's constant, h is the reduced Planck constant, m^* is the density-of-state effective mass of electrons and γ is the scattering factor.

Expression (1) shows that higher n decreases the S value, while larger γ increases the Seebeck coefficient. Normally, increase of ρ is accompanied by increase of S . But, Fig. 3(a) shows an opposite trend. So, the possible changes of m^* and γ in addition to the change of n should be taken into account to explain the S behavior of Bi_2Te_3 at the Lu or Tm doping. The value of γ is determined by mechanism of the charge carriers scattering. According to Fig. 2, this mechanism is the same for all

the compounds. So, γ will be the same, too. The value γ is equal to $-1/2$ for acoustic phonon scattering and to 0 for optical phonon scattering above the Debye temperature [28,29]. As was discussed above, both optical and acoustic phonon scattering should be considered as dominant mechanisms to explain the $\rho(T)$ behavior in Fig. 2. Therefore, for further analysis of S , let us assume that $\gamma = -1/2$ (acoustic phonon scattering) + 0 (optical phonon scattering) = $-1/2$. Next, in accordance with expression (1), a rate of the linear $S(T)$ growth in Fig. 3(a) can be characterized by a coefficient $\Delta S[\mu\text{V}\cdot\text{K}^{-1}]/\Delta T[\text{K}] \approx 2.14 \cdot 10^{-7}$. Using the values of n (Table 2), $\Delta S/\Delta T$ and γ , the density-of-states effective mass of electrons can be estimated. The estimates of m^* are given in Table 2 (m_0 is mass of free electron). So, at the doping m^* substantially increases from $0.16m_0$ for undoped Bi_2Te_3 up to $0.25m_0$ for $\text{Bi}_{1.9}\text{Lu}_{0.1}\text{Te}_3$ and $\text{Bi}_{1.9}\text{Tm}_{0.1}\text{Te}_3$. Increase of m^* can be related to forming the narrow impurity Lu or Tm band with the high and sharp DOS near the Fermi level. In this case, the energy band created by the impurity can lie in conduction band creating the resonant levels and local maximum in the electronic DOS, so that m^* can be improved without any effect on the mobility. As was mentioned above, enhancement in the thermoelectric properties due to increase in the electronic DOS was previously theoretically predicted [13].

The $k(T)$ dependences for Bi_2Te_3 , $\text{Bi}_{1.9}\text{Lu}_{0.1}\text{Te}_3$ and $\text{Bi}_{1.9}\text{Tm}_{0.1}\text{Te}_3$ measured by a laser flash method (a TC-1200 system) are presented in Fig. 3 (b). First, k decreases with increasing temperature for all the compounds. Second, the total thermal conductivity of doped Bi_2Te_3 is substantially lower compared to pure Bi_2Te_3 .

The $k(T)$ behavior can be attributed to the lattice thermal conductivity, k_p . Actually, it is known that at high temperatures above the Debye temperature k_p usually decreases with increasing temperature as T^{-1} [30]. This is because, phonon specific heat is a constant at high temperatures in accordance with the Pettit-Delong law, and phonon energy increases linearly with temperature, i.e. the number of phonons increases linearly with temperature. As the scattering rate is proportional to the number of phonons, the thermal conductivity decreases with increasing temperature.

Several mechanisms responsible for reducing the total thermal conductivity of Bi_2Te_3 at the Lu and Tm doping could be considered. First of all, the doping can introduce a number of the point defects in the Bi_2Te_3 lattice like the antisite defects and Lu atoms substituting for the Bi sites. These defects can reduce k_b by scattering phonons due to either mass contrast or local strains. For instance, theoretically, k of Bi_2Te_3 can be decreased down to 20% by the antisite defects [30]. Besides, the electronic contribution, k_e , to the total thermal conductivity should be taken into account. Due to k_e , decrease of ρ usually results in increase of k that is in contradiction with the change of ρ and k for our samples (Figs. 2 and Fig. 3(b)). The electronic thermal conductivity is related to the specific electrical conductivity, $\sigma = 1/\rho$, through the Wiedemann-Franz law $k_e = L\sigma T$ [31], where L is the Lorenz number. The Wiedemann-Franz law was originally developed for metals and its use for semiconductors can be limited. For metals, the Lorenz number is a constant equal to $2.45 \times 10^{-8} \text{ W}\Omega \text{ K}^{-2}$. The Wiedemann-Franz calculation of k_e for $\text{Bi}_{1.9}\text{Lu}_{0.1}\text{Te}_3$ and $\text{Bi}_{1.9}\text{Tm}_{0.1}\text{Te}_3$ gives an unacceptable conclusion that the electronic thermal conductivity is so great that the lattice thermal conductivity tends to zero, if the Lorenz number equal to $2.45 \times 10^{-8} \text{ W}\Omega \text{ K}^{-2}$ was assumed. It is important to note that the Wiedemann-Franz law cannot correctly distinguish the contributions from k_e and k_p in many semiconductors, in which the Lorenz number depends on carrier density and electron scattering [32].

Besides the Lu and Tm doping effect on the lattice thermal conductivity, reducing the electronic thermal conductivity was theoretically predicted for semiconductors with narrow impurity band with the high and sharp DOS near the Fermi level. Formation of such band originated from electronic $4f$ -levels of Lu or Tm was before assumed to explain the change of S at the doping (Fig. 3(a)). The physical reason for reduce of k_e is that as the heat carried by an electron is proportional to the difference between its energy and the Fermi energy and materials

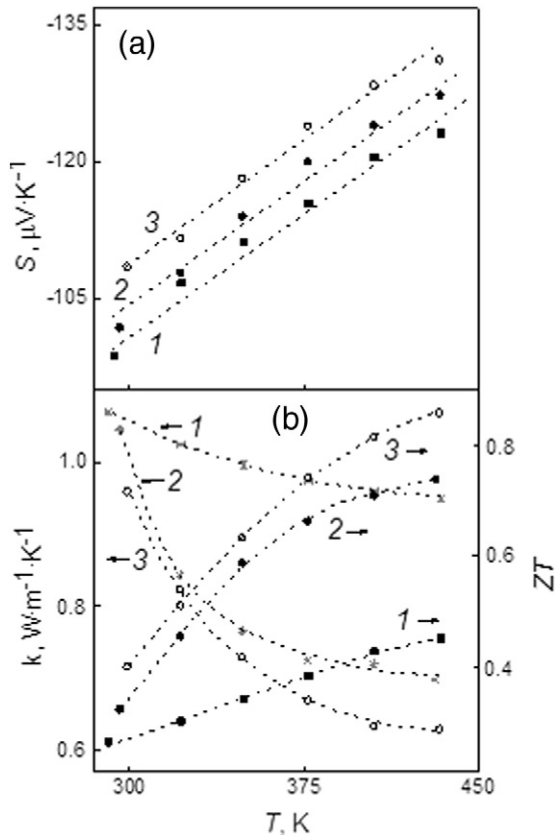


Fig. 3. (a) The $S(T)$ and, (b) $k(T)$ and $ZT(T)$ dependences for Bi_2Te_3 (curve 1), $\text{Bi}_{1.9}\text{Tm}_{0.1}\text{Te}_3$ (2) and $\text{Bi}_{1.9}\text{Lu}_{0.1}\text{Te}_3$ (3).

with narrow density of states ($\Delta E/2$ less than several $k_B T$, where ΔE is width of band), which “cut off” the high energy end of the Fermi distribution, have low k_e [12]. In this case, the Wiedemann-Franz law loses validity.

The $ZT(T)$ dependences for Bi_2Te_3 , $\text{Bi}_{1.9}\text{Lu}_{0.1}\text{Te}_3$ and $\text{Bi}_{1.9}\text{Tm}_{0.1}\text{Te}_3$ are also presented in Fig. 3(b). As is seen, the doping results in remarkable increase of ZT . Besides increase of the specific electrical resistivity, both increase of the Seebeck coefficient and decrease of the total conductivity are dominant sources resulting in enhancement of the thermoelectric figure-of-merit. Both increase of the density-of-states effective mass of electrons enhancing S and decrease of electronic thermal conductivity reducing k can be attributed to formation of narrow impurity Lu or Tm band with the high and sharp DOS near the Fermi level.

This work was supported by the Ministry of Education and Science of the Russian Federation (grant number No 3.6586.2017/BY).

References

- [1] G.J. Snyder, E.S. Toberer, *Nat. Mater.* 7 (2008) 105–114.
- [2] G. Mahan, B. Sales, J. Sharp, *Phys. Today* 50 (1997) 42–47.
- [3] T.M. Tritt, *Science* 283 (1999) 804–805.
- [4] Y.C. Lan, A.J. Minnich, G. Chen, Z.F. Ren, *Adv. Funct. Mater.* 20 (2010) 357–376.
- [5] X.K. Duan, K.G. Hu, D.H. Ma, W.N. Zhang, Y.Z. Jiang, S.C. Guo, *Rare Metals* 34 (2015) 770–775.
- [6] P. Srivastava, K. Singh, *Mater. Lett.* 136 (2014) 337–340.
- [7] B. Jarivala, D. Shah, N.M. Ravindra, *J. Electro. Dent. Mater.* 44 (2015) 1509–1516.
- [8] Y. Pan, T.R. Wei, C.F. Wu, J.F. Li, *J. Mater. Chem. C* 3 (2015) 10583–10589.
- [9] L. Hu, T. Zhu, X. Liu, X. Zhao, *Adv. Funct. Mater.* 24 (2014) 5211–5218.
- [10] J. Suh, K.M. Yu, D. Fu, X. Liu, F. Yang, J. Fan, D.J. Smith, Y.H. Zhang, J.K. Furdyna, C. Dames, W. Walukiewicz, J. Wu, *Adv. Mater.* 27 (2015) 3681–3686.
- [11] H.J. Goldsmid, *J. Electron. Mater.* 41 (2012) 2126–2129.
- [12] T.E. Hupphey, H. Linke, *Phys. Rev. Lett.* 94 (2015), 09660-1-4.
- [13] G.D. Mahan, J.O. Sofo, *Pros. Natl. Acad. Sci. USA* 93 (1996) 7436–7439.
- [14] J.P. Heremans, V. Jovovic, E.S. Toberer, A. Saramat, K. Kurosaki, A. Charoenphakdee, S. Yamanaka, G.J. Snyder, *Science* 321 (2008) 554–557.
- [15] M.D. Daybell, W.A. Steyert, *Rev. Mod. Phys.* 40 (1968) 380–389.
- [16] J. Yang, F. Wu, Z. Zhu, L. Yao, H. Song, X. Hu, *J. Alloys Compd.* 619 (2015) 401–405.
- [17] X.H. Ji, X.B. Zhao, Y.H. Zhang, B.H. Lu, H.L. Ni, *J. Alloys Compd.* 387 (2005) 282–286.
- [18] F. Wu, H. Song, J. Jia, X. Hu, *Prog. Nat. Sci. Mater. Int.* 23 (2013) 408–412.
- [19] F. Wu, W. Shi, X. Hu, *Electron. Mater. Lett.* 11 (2015) 127–132.
- [20] X.H. Ji, X.B. Zhao, Y.H. Zhang, B.H. Lu, H.L. Ni, *Lett* 59 (2005) 682–685.
- [21] F. Wu, H.Z. Song, J.F. Jia, F. Gao, Y.J. Zhang, X. Hu, *Phys. Stat. Sol. A* 210 (2013) 1183–1189.
- [22] W.Y. Shi, F. Wu, K.L. Wang, J.J. Yang, H.Z. Song, X.J. Hu, *Electron. Mater.* 43 (2014) 3162–3168.
- [23] X.B. Zhao, Y.H. Zhang, X.H. Ji, *Inorg. Chem. Commun.* 7 (2004) 386–388.
- [24] Y.Q. Jia, *J. Solid State Chem.* 95 (1991) 184–187.
- [25] D.C. Look, D.K. Lorance, J.R. Sizelove, C.E. Stutz, K.R. Evans, D.W. Whitson, *J. Appl. Phys.* 71 (1992) 260–266.
- [26] H.S. Bennett, *J. Appl. Phys.* 80 (1996) 3844–3853.
- [27] S.S. Li, in: S.S. Li (Ed.), *Semiconductor Physical Electronics*, Springer, New York 2006, pp. 211–245.
- [28] W.S. Liu, L.D. Zhao, B.P. Zhang, H.L. Zhang, J.F. Li, *Appl. Phys. Lett.* 93 (2008), 042109-1-4.
- [29] W. Liu, X. Yan, G. Chen, Z. Ren, *Nano Energy* 1 (2012) 42–56.
- [30] K. Termentzidis, O. Pokropyvnyy, M. Woda, S. Xiong, Y. Chumakov, P. Cortona, S. Volz, *J. Appl. Phys.* 113 (2013), 013506-1-7.
- [31] S. Wang, J. Yang, T. Toll, J. Yang, W. Zhang, X. Tang, *Sci. Report.* 5 (2015), 10136-1-9.
- [32] C.M. Bhandari, D.M. Rowe, *J. Phys. D. Appl. Phys.* 18 (1985) 873–884.